

Impact of swell on simulations using a regional atmospheric climate model

By BJÖRN CARLSSON*, ANNA RUTGERSSON and ANN-SOFI SMEDMAN, *Department of Earth Sciences, Meteorology, Uppsala University, Villavägen 16, SE-752 36 Uppsala, Sweden*

(Manuscript received 16 October 2008; in final form 16 March 2009)

ABSTRACT

When long, fast swell waves travel in approximately the same direction as the wind, the surface stress is reduced compared with under wind-sea conditions. Using measurements from the Östergarnsholm site in the Baltic Sea, new expressions of the roughness length were developed for wind sea and swell. These new expressions were implemented in the RCA3 regional climate model covering Europe. A 3-year simulation and two case studies using the wavefield from the ECMWF reanalysis (ERA-40) were analysed using the improved formulations. Wind-following swell led to a significant reduction of mean wind stress and heat fluxes. The mean surface layer wind speed was redistributed horizontally and the marine boundary layer cooled and dried slightly. This cooling was most pronounced over North Sea and the Norwegian Sea (almost 0.2°C annually on average) whereas the drying was most pronounced over the Mediterranean Sea (almost 0.4 g kg⁻¹). Somewhat less convective precipitation and low-level cloudiness over the sea areas were also indicated, in particular over the Mediterranean Sea. The impact on the atmosphere, however, is significantly locally greater in time and space.

1. Introduction

When modelling the atmosphere, it is crucial to describe the boundary conditions correctly. The atmosphere–ocean boundary is an important source of turbulence and is the site of significant exchange of momentum, heat and moisture. The marine atmospheric boundary layer (MABL) has a considerable impact on global climate models, since 70% of the global surface is covered with water.

There is a fundamental difference between the atmospheric boundary layer over land versus over sea. Over sea, the surface is not solid but changes in response to atmospheric forcing since surface waves are driven mainly by wind. The layer directly influenced by the waves is called the wave boundary layer (WBL). Above this layer, the same theories, as are valid over land, should hold (Edson and Fairall, 1998).

The atmospheric surface layer has traditionally been described by Monin–Obukhov similarity theory (MOST), which assumes stationary and homogeneous conditions and a solid surface. Numerous field measurements have confirmed the applicability of MOST over land (e.g. Businger et al., 1971; Haugen

et al., 1971; Högström, 1990) and over the ocean (Edson and Fairall, 1998). However, several investigations of the marine surface layer have found important deviations in the applicability of MOST (Smedman et al., 1994, 1999; Rutgersson et al., 2001).

Above the viscous sublayer, the total wind stress or momentum flux, τ , can be expressed as

$$\tau = \tau_t + \tau_w = \rho_a u_*^2. \quad (1)$$

Here, τ_t is the turbulent part, τ_w the wave-induced part and ρ_a is the air density; $u_* = ((-\overline{u'w'})^2 + (-\overline{v'w'})^2)^{1/4}$ is the measured friction velocity, with u' , v' , w' being the longitudinal, lateral and vertical wind fluctuations, respectively, and overbar denoting Reynolds average.

In models, the wind stress is generally described by a bulk formulation, the friction velocity being related to the wind speed by a bulk coefficient according to

$$\frac{\tau}{\rho_a} = u_*^2 = C_D U_{10}^2, \quad (2)$$

where C_D is the drag coefficient and U_{10} is the mean wind speed at 10 m above mean sea level.

The drag coefficient is a function of the roughness length, z_0 , atmospheric stability and the boundary layer height (Johansson et al., 2003). The neutral drag coefficient, C_{DN} , is defined here as a function of z_0 only. A smoother surface yields a smaller

*Corresponding author.

e-mail: Bjorn.Carlsson@met.uu.se

DOI: 10.1111/j.1600-0870.2009.00403.x

C_{DN} . Several studies of the bulk parameter find C_{DN} to be wind speed-dependent to a large extent (e.g. Large and Pond, 1981; Fairall et al., 2003).

An alternative way to calculate z_0 and thus C_{DN} is to use the Charnock expression (Charnock, 1955):

$$z_0 = \alpha \frac{u_*^2}{g}, \quad (3)$$

where α is the Charnock parameter and g the gravitational acceleration. This expression is used over sea in many atmospheric models. The fact that C_{DN} is dependent on wind speed is in agreement with eq. (3), since u_* is dependent on U_{10} . Some studies find that α and C_{DN} are dependent on the state of the waves as well (e.g. Stewart, 1974; Drennan et al., 2003; Carlsson et al., 2009).

Several previous studies investigated the impact of waves on the atmosphere, using coupled wave and atmospheric models. Doyle (1995) showed that waves had great impact on the development of depressions and Janssen and Viterbo (1996) that they affected atmospheric climate. In models, it has been demonstrated that including waves in the simulations influences the development of intense systems, such as tropical cyclones (Doyle, 2002). Lionello et al. (1998) simulated a depression and showed that the turbulent fluxes are sensitive to the wavefield, whereas the sea level pressure is not; they argue that at the beginning of cyclone development, the surface fluxes are of secondary importance. The outputs of both wave and atmospheric models were improved when they included wave-dependent wind stress. The above-mentioned investigations all focus on wind sea, that is, developing sea waves. However, very few previous investigations have simulated the effect of the relatively strong reduction of stress when long and fast waves, swell, travel in the same direction as the wind.

Simulations made using the RCA regional atmospheric climate model indicated that compared with measured values, wind stress was underestimated for high wind speeds and overestimated for low wind speeds (Ohlson, 2006). The overestimation of the stress could mainly be traced to occasions of wind-following swell.

The present study develops new empirical parametrizations for the Charnock coefficient, α , taking the wave effect into account. Data are from a measurement site in the Baltic Sea. The parametrizations are implemented and tested in the RCA regional atmospheric climate model to investigate the sensitivity of the model to the effect of waves.

Section 2 presents basic atmospheric surface-layer theory together with the effects of waves. The measurements and model are described in Section 3. The new parametrizations of α and the effect of the model implementation are presented in Section 4. In Section 5, a discussion is held about the wind gradient and suggested further research. Finally, a summary and some conclusions are given in Section 6.

2. Theory

2.1. Basic atmospheric surface-layer theory

According to MOST, the wind speed profile is related to the friction velocity:

$$U = \frac{u_*}{\kappa} \left[\ln \frac{z}{z_0} - \psi_m \right], \quad (4)$$

where $\kappa = 0.4$ is von Karman's constant, z height and ψ_m the integrated non-dimensional wind gradient (Paulson 1970) defined as

$$\psi_m(\zeta) = \int_0^\zeta \frac{1 - \phi_m(\zeta)}{\zeta} d\zeta, \quad (5)$$

where

$$\phi_m = \frac{\partial U}{\partial z} \frac{\kappa z}{u_*} \quad (6)$$

is the non-dimensional wind gradient. Höögström (1996) recommended that unstable atmospheric stratification over land be formulated thus:

$$\phi_m = (1 - 19\zeta)^{-1/4}. \quad (7)$$

The stability parameter ζ is defined as

$$\zeta = \frac{z}{L} = -\frac{zg\kappa \overline{w'\theta'_v}}{u_*^3 T_0}, \quad (8)$$

where L is the Obukhov length, $\overline{w'\theta'_v}$ is the buoyancy flux (kinematic flux of virtual temperature) and T_0 the mean temperature in the surface layer; $\zeta < 0$ indicates that the stratification is unstable. Under neutral conditions $\psi_m = 0$, and eq. (4) reduces to the logarithmic law of the wall.

The neutral drag coefficient is given by

$$C_{DN} = \left(\frac{\kappa}{\ln \frac{10}{z_0}} \right)^2. \quad (9)$$

Using eqs. (2), (4) and (9), the stability-influenced drag coefficient is

$$C_D = \left(\frac{\kappa}{\sqrt{C_{DN}} - \psi_m} \right)^2. \quad (10)$$

2.2. Effect of waves on the atmospheric surface layer

The state of the waves can be described by wave age, that is, c_p/U_{10} or c_p/u_* , where c_p is the phase speed of the dominant waves. Phase speed and frequency, n , are related by the dispersion relation:

$$c = \frac{g}{2\pi n} \tanh \frac{2\pi nd}{c}, \quad (11)$$

which includes iteration. In deep water (water depth, d , being greater than half the wavelength), relation (11) reduces to $c = g/2\pi n$. The definition c_p/u_* is more convenient in an

atmospheric model, as U_{10} is a diagnostic parameter and 10 m above mean sea level is not a level used in the model simulations made in this investigation.

According to Pierson and Moskowitz (1964) and Pierson (1964) the wave age at which the waves are fully developed is $c_p/U_{10} = 1.2$ (this refers to $c_p/u_* \approx 35$). The two wave states are described by the following:

wind sea, that is, $c_p/U_{10} < 1.2$,

and swell, that is, $c_p/U_{10} > 1.2$.

Wind sea comprises relatively short, slow waves produced locally by wind. Then the WBL is of the order of 1 m thick, and measurements indicate limited wave impact on the atmosphere. Several investigations have focused on this regime (e.g. Drennan et al., 2003; Hwang, 2005). During wind sea, it is easier to describe the surface roughness, as the waves are more or less a function of the local wind speed and fetch.

Swells are long waves not in scale with the present local wind input. This is often the case during a decaying storm or when long waves are transported from a distant storm. Since swell can travel long distances without dissipating, it has been assumed that there is no transport of energy from the waves to the wind. During swell, however, the WBL is significantly deeper and the structure in the whole boundary layer could be affected (Smedman et al., 1994, 1999). That swell affects the turbulence structure of the overlying airflow, is supported by measurements and by the results of direct numerical simulation (Sullivan et al., 2000; Rutgersson and Sullivan, 2005) and large eddy simulation (LES) (Sullivan et al., 2008).

The definition of wave age sometimes includes the factor $1/\cos \beta$ (e.g. Donelan et al., 1985), where β is the angle between the local wind and the waves. Using this would produce unrealistic results for swell waves, since this factor can be very large for such waves. This would imply increasing atmospheric effects with increasing values of $1/\cos \beta$, which is not in line with our data for the approximate range of $\beta < 90^\circ$ (Carlsson et al., 2009). As a result, we choose not to include the $1/\cos \beta$ factor here.

In most investigations analysing measurements made during swell, the scatter of C_{DN} increases significantly compared with that under wind-sea conditions. When the swell direction follows the wind direction (i.e. wind-following swell), the drag coefficient is reduced (Drennan et al., 1999; Guo Larsén et al., 2003; Carlsson et al., 2009). When the swell direction is across or against the wind direction (cross/counter swell), C_{DN} has been seen to increase (Drennan et al., 1999; Guo Larsén et al., 2003; Pan et al., 2005). This can be explained by τ_w , which contributes with upward momentum transport during wind-following swell, that is, wave energy is transported from the waves to the wind. The turbulent contribution, τ_t , always gives a negative (downward) momentum transport, and for further increase of the wave age, there can be a sign reversal of $\tau_t + \tau_w$, that is, a net positive upward momentum transport (Smedman et al., 1999; Grachev and Fairall, 2001). Other deviations from MOST observed in the presence of swell include a low-level wind maxi-

mum (e.g. Holland et al., 1981; Donelan, 1990; Rutgersson et al., 2001).

Guo Larsén et al. (2004) found that ϕ_m is a function of the state of the waves. For wind sea ($c_p/U_{10} < 1.2$) and under unstable conditions, one can use eq. (7); for wind-following swell ($c_p/U_{10} > 1.2$), one can use the following:

$$\phi_m = 1 - (-3\zeta)^{-1/2}, \quad -1 < \zeta < 0, \quad (12a)$$

$$\phi_m = -0.73, \quad \zeta < -1. \quad (12b)$$

Following Drennan et al. (2003), the Charnock parameter in the Charnock relation (3) can be expressed as

$$\alpha = a \left(\frac{c_p}{u_*} \right)^b, \quad (13)$$

where a is positive and b is negative.

Sometimes a smooth flow term is added to the expression of z_0 :

$$z_0 = \alpha \frac{u_*^2}{g} + 0.11 \frac{\nu}{u_*}. \quad (14)$$

The second term determines the smooth flow contribution at low wind speeds, ν being the dynamic viscosity of air.

3. Measurements and model

3.1. Site and instrumentation

The measurements used in this investigation were made at the field station on the island of Östergarnsholm. Östergarnsholm, situated approximately 4 km east of Gotland in the Baltic Sea (at A in Fig. 1a), has few trees and is very flat. A 30-m-tall measurement tower has been erected at the southernmost tip of the island, with its base at approximately 1 m above mean sea level. For the wind directions 80° – 220° , the data obtained from this tower have been shown to represent marine conditions (Smedman et al., 1999). In a previous analysis of the wavefield disturbance in combination with a footprint analysis, Smedman et al. (1999) showed that the limited near-shore water depth in the vicinity of the tower had a very small impact on the measurements. Högström et al. (2008) demonstrated that measurements made from the tower correctly represented conditions in the footprint area.

Mean profile data were obtained from slow-response instruments measuring wind speed, wind direction and temperature at five levels (8, 12.5, 15, 21 and 29 m above mean sea level) and humidity at one level (8 m). Turbulence was calculated using data from Solent 1012R2 sonic anemometers (Gill Instruments, Lymington, UK) at three heights (10, 18 and 26 m) measuring sonic temperature and the three wind components and sampling at 20 Hz.

A wave-rider buoy (run and owned by the Finnish Institute of Marine Research), moored 3.5 km in the direction of 115°

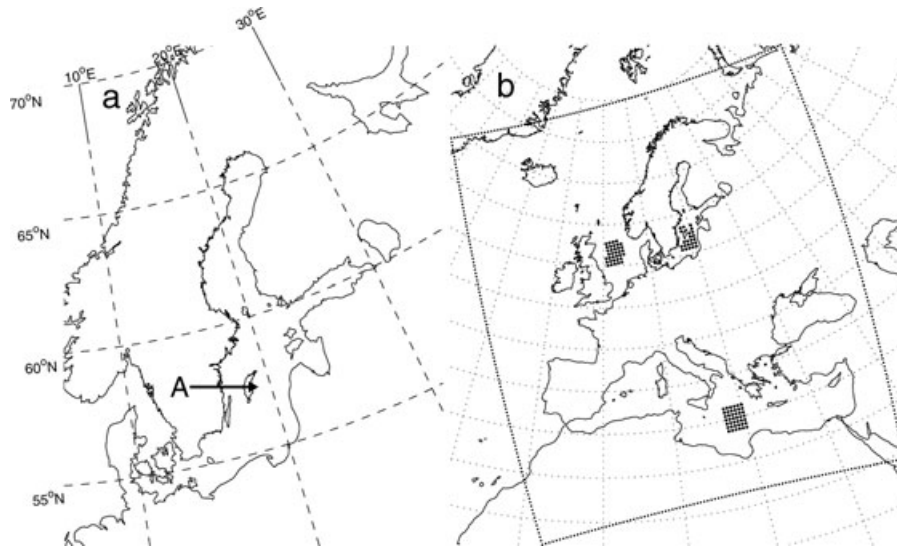


Fig. 1. (a) Close-up view of the Baltic Sea; arrow 'A' indicates the location of the Östergarnsholm site. (b) The RCA model domain area is enclosed by the dotted frame. Dotted areas (i.e. the Baltic, North and Mediterranean seas) are analysed in detail in Section 4.3.

from the tower, measures the wavefield and sea surface temperature (SST). Wave phase speed is weighted according to a footprint weighting function given in Smedman et al. (1999). The deep-sea dispersion relation (eq. 11) is used for $c_p < 6.5 \text{ m s}^{-1}$; otherwise, eq. (5) in Smedman et al. (2003) is used. For a more detailed description of the site and instrumentation, see Smedman et al. (1999).

Data were selected according to the following criteria: wind from the $80\text{--}220^\circ$ sector, wind speed above 2 m s^{-1} , only upward sensible flux (unstable stratification), and a dominant wavefield from the $40\text{--}210^\circ$ sector. Turbulent fluxes were calculated using the eddy-correlation method and all turbulence statistics were expressed as a 10-min running average to remove trends. For swell data, filtering was applied to the momentum flux (Carlsson et al., 2009). The filtering separates the irregular low-frequency variations from the turbulence fluctuations generating stress under swell conditions. Data were calculated as hourly averages for the 1995–2004 period; at least 30 min of data were used in calculating each hourly average. Maximum wind speed was just above 15 m s^{-1} .

3.2. Model

The Rossby Centre atmospheric regional climate model, version 3 (RCA3) has been developed at the Swedish Meteorological and Hydrological Institute (SMHI) and its domain includes Europe (Fig. 1b). It is a hydrostatic model, incorporating terrain-following coordinates, semi-Lagrangian semi-implicit calculations, and a 30-min time step; the horizontal resolution is 0.44° (approximately 50 km) and the model is vertically resolved in 24 levels up to 10 hPa. In the present study, the model is forced at the lateral boundaries and the lower boundary, that is, SST and ice, by ECMWF reanalysis data (ERA-40). This study also uses

phase speed and direction of dominant waves from the same data set, calculated using the WAM model (WAMDI Group, 1988). Surface-layer relationships according to MOST are used below the lowest model level at 90 m above mean sea level to calculate the wind speed at 10 m and temperature and specific humidity at 2 m. The turbulent fluxes are calculated according to Woetmann-Nielsen (1998), with some minor changes (see appendix B and eqs. 12a–15) in Rutgersson et al., 2007). The roughness length in the original version of the RCA model is described by

$$z_0 = f(U) \times \alpha \frac{u_*^2}{g} + [1 - f(U)] \times 0.11 \frac{\nu}{u_*}, \quad (15)$$

where α is set to 0.014 and 0.032 over open and coastal water, respectively, and f is a wind speed weighting function for the transition between smooth and rough flow. The wind stress is achieved in the model using a drag coefficient (eqs. 9–10) calculated for the lowest model level (C_{D90}), instead of 10 m. For more detailed information regarding the RCA model and its components, see, for example, Jones et al. (2004).

4. Results

4.1. Parametrization of Charnock parameter

For the parametrization of the Charnock parameter, α , we focus on the unstable data, since the influence of swell is not significant for stable data (Rutgersson et al., 2001). According to Rutgersson et al. (2001), the stability parameter, ζ , ceases to be a relevant scaling parameter during swell. This is because u_* approaches zero during swell, giving large negative values of ζ even if the heat/buoyancy flux is small. For swell data, $\zeta = -0.4$ was set as a lower limit for the stability-dependent C_D . To avoid the impact of spurious correlation, we developed an expression

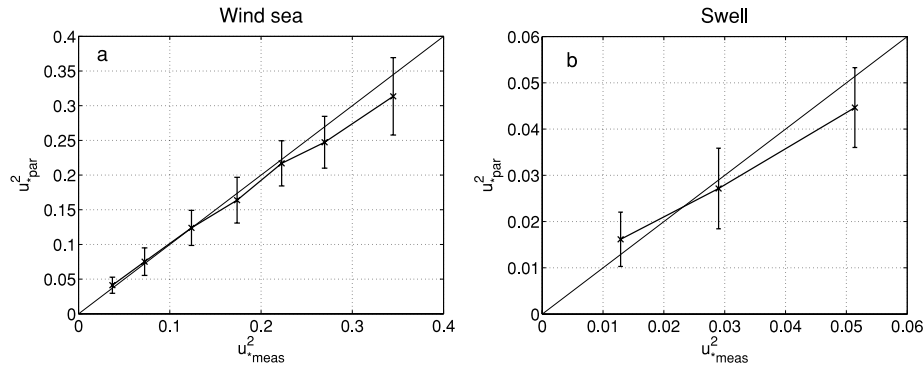


Fig. 2. Calculated u_*^2 plotted against measured u_*^2 during (a) wind sea and (b) swell. Bars indicate the standard deviation.

for α (eq. 13), giving the best agreement between measured and calculated values of u_* . This was done by tuning the a and b parameters in eq. (13). The u_* was calculated using eqs. (2), (5), (8)–(10), (13) and (14). The non-dimensional wind gradient ϕ_m was given by eq. (7) or eq. (12a) for wind sea or swell, respectively. This parametrization of α gives weaker wave age dependence compared with when using a simple best fit between wave age and α , since lower weight is given to extreme values in the present method.

The data for wind-sea conditions ($c_p/U_{10} < 1.2$ and $c_p/u_* < 35$) cover 448 h and the resulting parametrized expression reads

$$\alpha = 0.03 (c_p/u_*)^{-0.4}. \quad (16)$$

Figure 2a shows the calculated u_*^2 plotted against the observed values for wind sea. As the method gives a lower weight to extreme values, underestimations for high observed values of u_*^2 were allowed and vice versa. The correlation coefficient, r , for this parametrization is 0.95. There were few wind-sea cases with a wind speed below 5 m s^{-1} ; so, the smooth flow term in eq. (14) could not be investigated. On average, α is close to 0.009 in this expression.

The relatively small wave age dependence found here for C_{DN} was explained in Smedman et al. (2003), who demonstrated that z_0 (through α) is not governed solely by wave age but by two parameters representing the wave state, that is, wave age and E_1/E_2 ; E_1 and E_2 are defined as the energy of long and short waves, respectively. Thus, for wind sea, the relative energy of the long (fast) and short (slow) waves is an important parameter in combination with wave age. When lacking information about this parameter, we suggest using the weak wave age dependence given by eq. (16).

There are 197 h of data available that include swell conditions ($c_p/U_{10} > 1.2$ and $c_p/u_* > 35$). In line with the results of Carlsson et al. (2009), the wind-following swell term is henceforth used for $\beta < 90^\circ$. A parametrization was developed especially for this kind of swell. The second term in eq. (14) was omitted, arriving at eq. (3) instead, as the smooth flow enhancement of z_0 under swell conditions is not expected. The resulting

expression is

$$\alpha = 0.0021 (c_p/u_*)^{-0.4}. \quad (17)$$

This means that α is close to 0.00045 in this expression. Figure 2b shows the resulting u_*^2 plotted as calculated values versus observed values for wind-following swell. As found in other studies, the scatter in the data is larger than for wind-sea conditions and the correlation coefficient, r , for the expression is 0.81.

To compare our parametrizations (eqs. 16–17) with those of previous studies of C_{DN} , we use the new expressions of α and parametrize the measured wave age as a function of wind speed. Corresponding C_{DN} values can be calculated using eqs. (3) and (9). Figure 3 shows these expressions (solid lines, see legend), together with our measurements (dashed lines, see legend) and the widely used Couple Ocean–Atmosphere Response Experiment (COARE) 3.0 (dashed-dotted line) expression of Fairall et al. (2003). In contrast, the present study arrives at somewhat

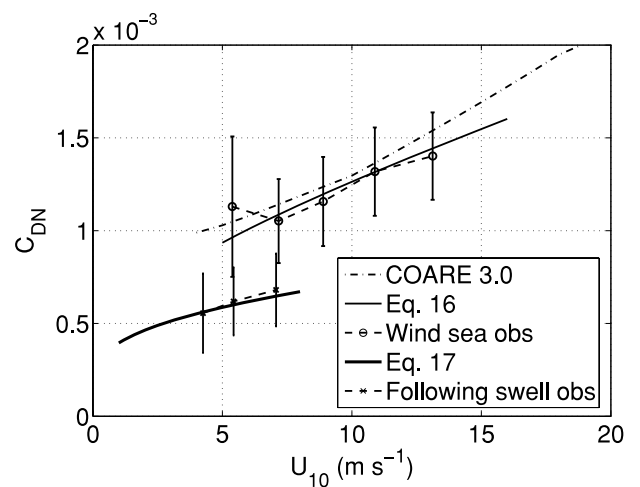


Fig. 3. The neutral drag coefficient as a function of wind speed. The wave age information in eqs. (16) and (17) are calculated from a wave age–wind speed relation found in the measurements. Error bars indicate the standard deviation of the measurements.

smaller values for wind-sea conditions. The swell expression gives approximately half the wind-sea value. Guo Larsén et al. (2003) partly used the same data set (using data from the 1995 to 1998 period), and their result for swell conditions is close to ours. The C_{DN} expressions developed in Carlsson et al. (2009) produce results close to the current parametrization of α .

4.2. Implementation of the new Charnock parameter in the RCA model

As originally set up, RCA3 uses $\alpha = 0.014$. It is assumed that several constants in RCA3 are tuned to that value of α and are valid for wind sea. Since our aim is to investigate the effect of swell in the model, we choose to apply the wave age dependence from eq. (16) and (17) but scale these equations by 1.6 (dividing the original $\alpha = 0.014$ with the mean wind sea $\alpha = 0.009$ obtained in this study). It was shown in Smedman et al. (2003) that the background amount of swell waves (described by the parameter E_1/E_2) enhances z_0 . It is most likely that for large sea areas like the Atlantic Ocean and the Mediterranean Sea E_1/E_2 is larger than in the Baltic Sea and thus α as well.

Thus, the expressions used in the model are for wind sea and cross/counter swell:

$$\alpha = 0.05 (c_p/u_*)^{-0.4}, \quad (18)$$

and for wind-following swell:

$$\alpha = 0.0035 (c_p/u_*)^{-0.4}. \quad (19)$$

A linear interpolation of α is, however, done between eqs. (18) and (19) in the region $30 < c_p/u_* < 40$ to avoid singularities. When calculating z_0 during swell in the model, eq. (3) is used instead of eq. (15).

4.3. Model results

As our expressions of roughness during swell were developed for conditions over the Baltic Sea, their validity is most certain when only applied over the Baltic Sea. However, swell conditions are even more common over the open ocean, where the wavefield is often more complex than in Baltic Sea, where swell comes from only one direction at a time. We choose here also to extrapolate our findings to all ocean parts of the domain, even though more study is needed to parametrize the wind stress valid for wind-following swell over the open ocean. The stability parameter, ζ , is limited during swell, as in the parametrization procedure in Section 4.1.

Three simulations were performed and are denoted as follows:

REF (reference)	New wind sea expression (eq. 18)
SW	New swell expression (eq. 19) for wind-following swell (unstable stratification); otherwise wind sea expression (eq. 18)
SWBAL	As in SW, but the swell expression (eq. 19) was included only for Baltic Sea

The impact of the new swell parametrization was investigated in a 3-year simulation (1995–1997) and two case studies.

Detailed analyses of three areas, that is, the Mediterranean, southern Baltic and North seas (indicated by dotted areas in Fig. 1), were done; the results presented below are area averages.

For the simulation with the swell expression used only in the Baltic Sea (SWBAL), the impact of swell in the southern Baltic Sea reduces the mean wind stress by 2.5%, from 0.085 (REF) to 0.083 $N m^{-2}$. For swell cases (hereafter defined as $c_p/u_* > 30$ and unstable stratification) in the analysis, the reduction of wind stress is 16% or 0.007 $N m^{-2}$. In Figs. 4a–f, the seasonal variation of differences in fluxes, wind speed, temperature and humidity are shown for swell conditions. Wind stress exhibits the largest mean decrease, $-0.01 N m^{-2}$, in winter (for swell conditions) but also an increase in May (dashed curve in Fig. 4a). This is because swell events with unstable stratification mainly occur in autumn and winter (Fig. 5a). Guo Larsén (2003) found the wave age ($c_p/u_* > 30$) for 55% of the time at Östergarnsholm, under all stability conditions. This value is close to the yearly value for the southern Baltic Sea (60%) given by the model and the ERA-40 wavefield. An influence on the sensible and latent heat fluxes also results in smaller upward fluxes; this is partly due to the changed z_0 , which also influences the exchange coefficients for the heat fluxes. The decrease during swell in these exchange coefficients is in agreement with measurements in Smedman et al. (2007). The sensible heat flux is reduced from 8.9 to 8.3 $W m^{-2}$ (7%) and the latent heat flux from 41.9 to 39.5 $W m^{-2}$ (6%). When only investigating cases in which swell is present, the sensible and latent fluxes are reduced by 1.8 and 7.4 $W m^{-2}$ (16% and 17%), respectively. As with the momentum flux, the largest impact on heat fluxes is seen for the winter months (Figs. 4c and e showing swell conditions).

On average, the reduced fluxes (SWBAL) have only a small impact on wind speed, temperature and specific humidity (not shown). When only investigating cases in which swell is present, the change is somewhat greater for the wind speed at 10 m above mean sea level (dashed line in Fig. 4b), which is on average 0.1 $m s^{-1}$ higher. The increase in wind speed occurs throughout the MABL, up to a height of approximately 800 m (Fig. 6a). This is expected because reduced wind stress causes less friction.

When applying the swell effect on the roughness over the whole domain (SW), the changes in fluxes for the Baltic Sea region are almost the same as in the SWBAL run (solid lines in Figs. 4a, c and e). The MABL becomes approximately 0.1°C cooler (Fig. 6b) and 0.1 $g kg^{-1}$ dryer (solid lines in Figs. 4d and f). The wind speed increases at 10 m above mean sea level (Fig. 4b); higher up, however, the wind instead decreases somewhat (Fig. 6a), possibly due to stability effects and advection processes.

Swell conditions during unstable stratification are more common over the North Sea than the Baltic Sea (Fig. 5b). During swell, the average wind stress declines from 0.076 (REF) to 0.059 $N m^{-2}$ (22%), sensible heat flux from 12.8 to 12.2 $W m^{-2}$

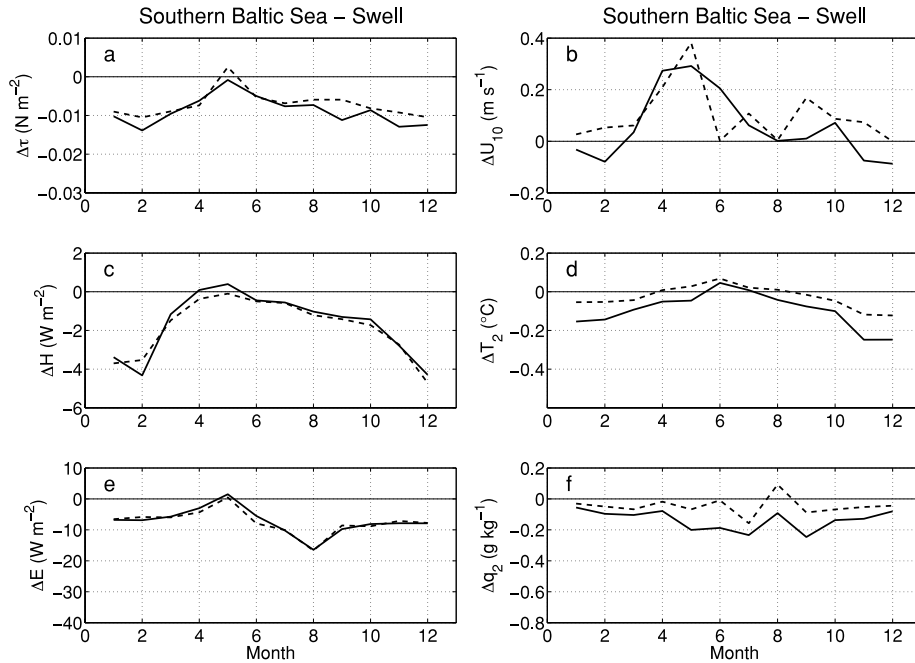


Fig. 4. Monthly mean differences in turbulent fluxes (left-hand side) and low-level wind speed, temperature and humidity (right-hand side) under swell and unstable conditions. The thick solid lines are the SW run minus the REF run and the dashed lines the SWBAL run minus the REF run. The thin solid lines correspond to zero difference.

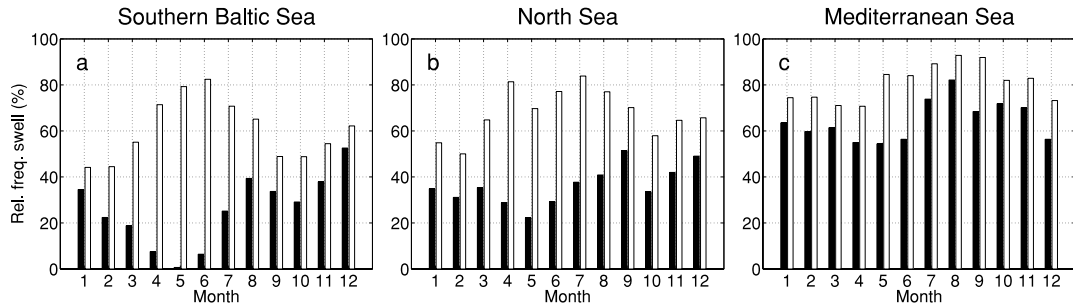


Fig. 5. Monthly distribution of swell cases ($c_p/u_* > 30$). The white bars include both unstable and stable stratification, whereas the black bars represent only unstable swell events.

(5%) and latent heat flux from 56.4 to 48.6 W m^{-2} (14%). There are smaller seasonal variations of the flux differences (Figs. 7a, c, and e) over the North Sea than the Baltic Sea. Wind speed at 10 m above mean sea level increases by approximately 0.1 m s^{-1} on average during swell (Fig. 7b), but higher up, the same reduction is seen as over the Baltic Sea (not shown). The MABL becomes an average of $0.2\text{--}0.3^{\circ}\text{C}$ colder and $0.1\text{--}0.3 \text{ g kg}^{-1}$ dryer during swell, with the largest impact at 2 m. There is a tendency toward more cooling in winter as well as more drying in autumn, when the specific humidity is higher than in winter (Figs. 7d and f).

In the part of Mediterranean Sea south of the Ionian Sea, the wind stress is reduced from 0.046 (REF) to 0.034 N m^{-2} (26%) during swell conditions. Swell conditions with unstable stratification are even more common here than in the North Sea (Fig. 5c). Sensible heat flux declines from 12.0 to 10.2 W m^{-2}

(16%) and latent heat flux from 108 to 87 W m^{-2} (20%). The same seasonal flux variations as seen for the North Sea are seen here, but are more pronounced (Figs. 8a, c and e). Wind speed change is close to zero near the surface (Fig. 8b), but higher up it declines as it does in the other areas. The MABL becomes on an average $0.1\text{--}0.2^{\circ}\text{C}$ colder and $0.3\text{--}0.4 \text{ g kg}^{-1}$ dryer, with the largest impact at 2 m (Figs. 8d and f). The greater drying here than in the northern areas can be explained by the higher temperatures and, thus, moister air in terms of specific humidity.

The above analysis of the three different areas indicates a colder (especially over the North Sea) and dryer (especially over the Mediterranean Sea) MABL, with slower winds except close to the surface. Is the same true outside these three areas? In Fig. 9, the model fields for the mean change (SW – REF, and all conditions) in wind speed, temperature and humidity at the lowest model level (approximately 90 m above mean sea

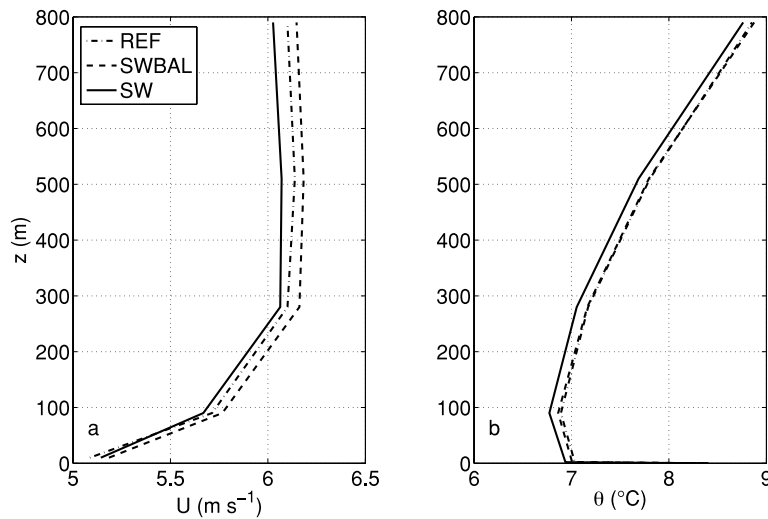


Fig. 6. Mean profiles of wind speed and potential temperature for all swell cases with unstable stratification over the southern Baltic Sea.

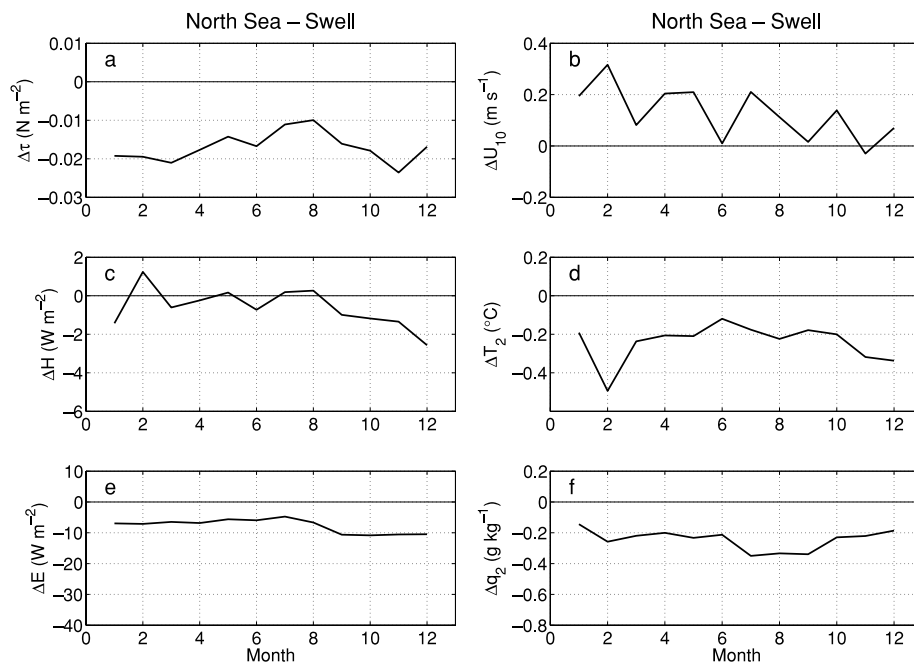


Fig. 7. Difference in turbulent fluxes (left-hand side) and low-level wind speed, temperature and humidity (right-hand side) under swell and unstable conditions. Solid lines indicate the SW run minus the REF run.

level) are shown together with the mean change in yearly precipitation. The 10 grid cells at the boundaries are removed in the following analysis of the simulations. The mean effect on the wind speed (Fig. 9a) is very slight, and there is a rather small redistribution. The mean temperature (Fig. 9b) decreases by 0.06°C over the domain, most significantly so over the North Sea and Norwegian Sea. Specific humidity (Fig. 9c) declines by 0.1 g kg^{-1} , the largest change being in the southern Mediterranean Sea, as indicated above. Precipitation is redistributed, several areas having 50 mm more or 50 mm less mean yearly precipitation (Fig. 9d). The precipitation reduction is mainly over the sea (in the Mediterranean Sea we find a 20% reduction)

and the increase, over land areas. Also, there is a significant mean reduction in precipitation of 20 mm (3%) over the entire domain due to reduced evaporation; the change is mainly in the convective precipitation.

Other changed parameters not shown here include low-level cloud cover, which is reduced by an average of 5% (from 13.6% to 13.1%) and by 20%–30% (from 5%–10% to 1–3 percentage points lower values) over the Mediterranean Sea. In addition, over the same area, the reduction in the mean mixed layer depth reaches its maximum, almost 50 m, whereas the mean turbulent kinetic energy (TKE) in the MABL declines by 5% in the eastern part of the Mediterranean Sea.

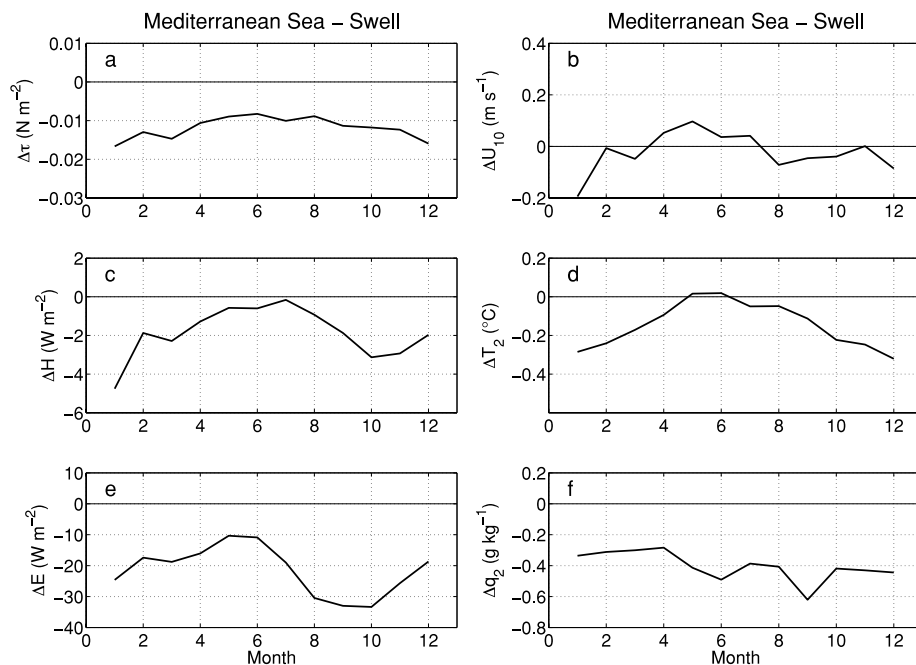


Fig. 8. Difference in turbulent fluxes (left-hand side) and low-level wind speed, temperature and humidity (right-hand side) under swell and unstable conditions. Solid lines indicate the SW run minus the REF run.

Two shorter periods were also simulated to investigate the swell impact on shorter timescales. From these, it is found that the swell impact on cyclonic development is minor, partly because of the relatively small area of swell. In high-pressure situations involving larger areas of swell and with unstable stratification, wind speed is redistributed, in some areas by more than 1 m s^{-1} . There is also a mean decrease in temperature and humidity (more than 1°C and 1 g kg^{-1}) in the swell areas, mainly due to changes in sensible and latent heat fluxes (mostly decreasing upward flux) and not to redistribution. Also, redistribution of both convective and large-scale precipitation can be seen.

If the grid size had been decreased, there is a possibility that the impact of swell would have been greater (cf. Janssen et al., 2001). One can also argue that if the RCA model had been coupled with a wave and ocean model, the effect would have been smaller because of the aim to achieve equilibrium between the model parts.

5. Discussion

This study has only dealt with the change of sea surface roughness due to the waves. Measurements indicate that both the turbulence structure and wind gradients change during swell. Changed wind gradients give changed ϕ_m functions (eqs. 7 and 12a). The ϕ_m expression used for swell was developed for a height of 10 m above mean sea level (Guo Larsén et al., 2004) and is perhaps not valid up to 90 m—the lowest model level. The non-dimensional gradient, ϕ_m , probably varies with both

wave state and height. Rutgersson et al. (2001) concluded that ϕ_m during swell agrees better with traditional expressions at 26 m than at 10 m, which means that the effect of swell on ϕ_m would decrease with height. Still, Smedman et al. (1994) found that, during swell, the wind speed was nearly constant from a few metres above sea level to heights of several hundred metres; this is also seen in LES (Sullivan et al., 2008). Figure 10 shows the calculated mean wind profiles from $U_{90} = 6 \text{ m s}^{-1}$ for a typical case with swell and slightly unstable stratification, using the values of ϕ_m valid for wind sea (eq. 7, solid curve) and for swell (eq. 12a, dashed-dotted curve). In the present study, U_{10} is calculated from U_{90} in the model using the wind-sea expression (due to the uncertainties in ϕ_m). More detailed study of the behaviour of the ϕ_m function is needed.

A correct expression of ϕ_m should probably combine eqs. (7) and (12a) and would also be a function of the boundary-layer height (Johansson et al., 2003). We can, in the absence of complete knowledge of ϕ_m , assume a constant wind speed (following Smedman et al., 1994) at heights between 10 and 90 m above mean sea level. If, for the present study, we assume $U_{10} = U_{90}$ (i.e. $\phi_m = 0$) during swell, the modelled wind speed at 10 m becomes higher. The mean increase in the three investigated areas (presented in Section 4.3) is $0.15\text{--}0.3 \text{ m s}^{-1}$. The increase under swell conditions averages $0.4\text{--}0.8 \text{ m s}^{-1}$.

In this study, there were not enough data to parametrize the enhancing effect of cross and counter swell on the roughness length. Future research into this and into their impact on an atmospheric model is crucial if we are to gain more complete understanding of the air–sea interaction of momentum.

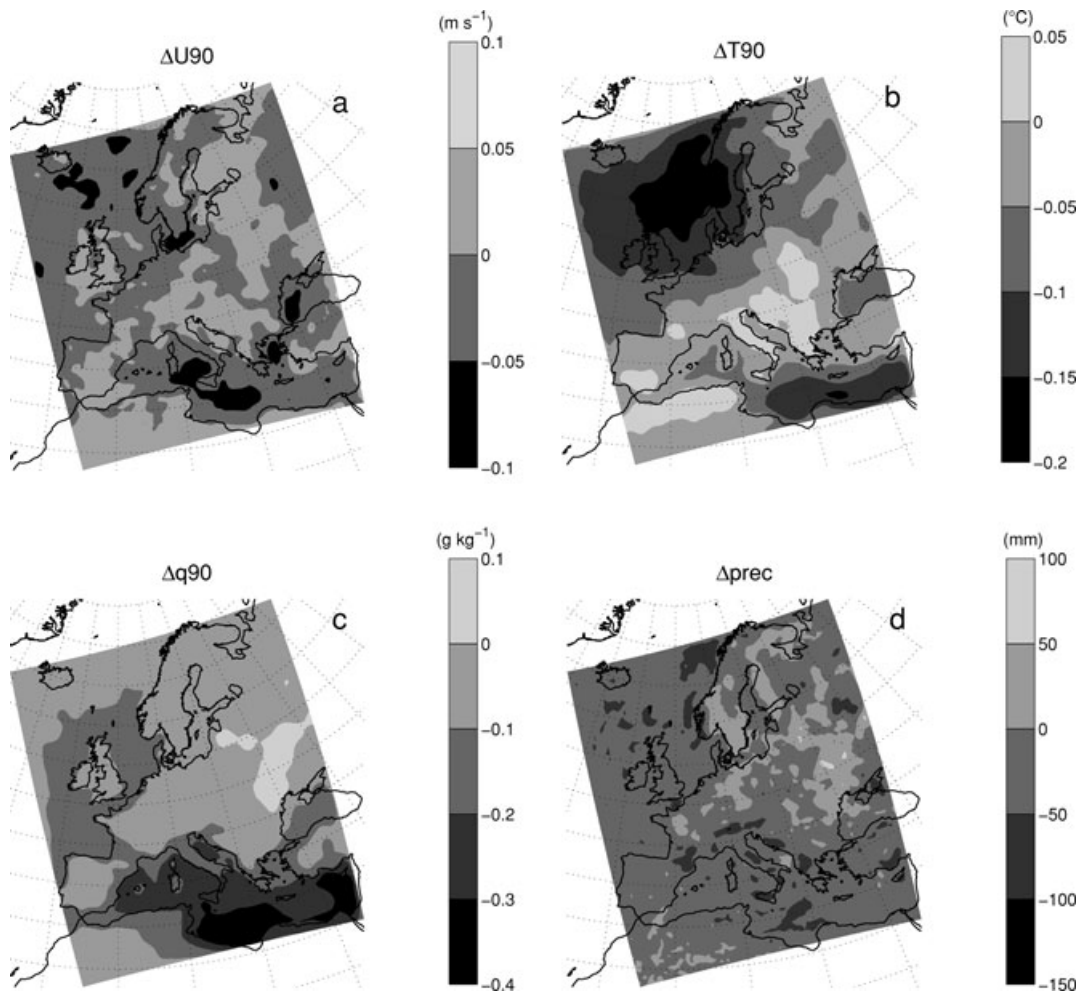


Fig. 9. Fields of yearly difference at the lowest model level and of precipitation (SW – REF). The 10 outer grid cells are excluded from the analysis.

6. Summary and conclusions

During swell, that is, when the dominant sea waves travel faster than the wind, the turbulence structure of the atmosphere changes compared with under wind-sea conditions or over land. Among other processes, the wind stress is altered. For wind-following swell, that is, wind and waves aligned within 90° , the stress is significantly lower than under wind-sea conditions.

Using measurements made in the Baltic Sea, two new expressions of the roughness parameter were developed for wind sea and wind-following swell. These new expressions were implemented in the RCA3 regional climate model, covering Europe, to investigate the atmospheric effects of the reduced wind stress due to swell. A 3-year analysis and two case studies were presented.

The main results are:

(1) As a 3-year average, the wind stress was reduced by 2%–12% due to swell, the highest values being in the Mediterranean Sea. When considering only swell situations, the stress was re-

duced by 20%–26%. The heat fluxes were also significantly reduced.

(2) There was area-average cooling (on the order of 0.1°C) and drying (on the order of 0.1 g kg^{-1}) of the MABL while wind speed was being horizontally redistributed. Mean low-level cloud cover was reduced by up to 30% over the Mediterranean Sea, and the local precipitation was reduced by more than 10% (convective), mostly over the sea areas.

(3) A case study of an area dominated by swell demonstrated that the impact on the atmosphere is locally greater in time and space (over 1 m s^{-1} and 1°C).

(4) Assuming constant wind speed of between 10 and 90 m s^{-1} during swell in the model, in line with observations, the wind speed at 10 m above mean sea level was enhanced by up to 0.3 m s^{-1} as a 3-year average.

To conclude, implementing the swell effect is mainly important to wind stress and heat fluxes (The limited swell effects on wind, temperature and humidity are probably due to the already small wind stress during swell, as wind speed is mainly low

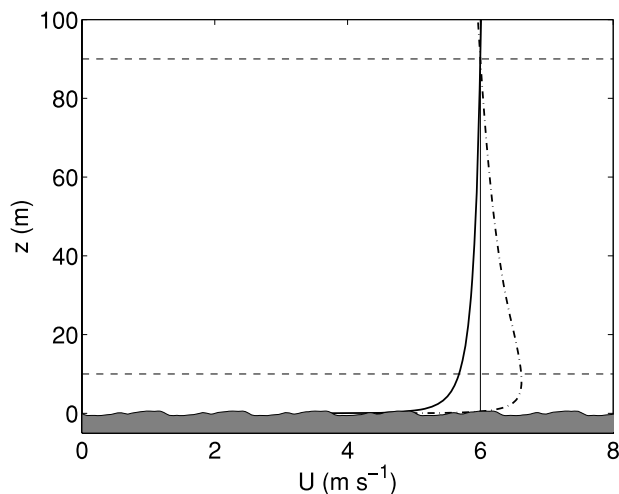


Fig. 10. Example of wind profile achieved by the ϕ_m function valid for wind sea (solid line) and wind-following swell (dashed-dotted line) calculated from U_{90} . Dashed horizontal lines indicate the lowest model level (90 m above mean sea level) and the height of measurements (10 m).

under these conditions). Swell has significantly different impacts in different areas and could possibly affect circulation patterns in a global model. To include all swell effects, further investigation is needed to implement the changed turbulence structure evident in observations made under swell conditions.

7. Acknowledgments

The authors wish to thank Kimmo Kahma and Heidi Pettersson at the Finnish Institute of Marine Research, Helsinki, Finland, for the wave and water temperature data and Erik Sahlée and Ulf Högström at the Department of Earth Sciences, Uppsala University, Sweden, and Xiaoli Guo Larsén at the Wind Energy Division, National Laboratory for Sustainable Energy, Roskilde, Denmark, for the development of the database. The Rosby Centre, SMHI is acknowledged for providing access to the RCA model; special thanks to Anders Ullerstig at SMHI for valuable help with the model and the output and for preparing the wave input from ERA-40 data.

References

- Businger, J. A., Wyngaard, J. C., Izumi, Y. and Bradley, E. F. 1971. Flux-profile relationships in the atmospheric surface layer. *J. Atmos. Sci.* **28**, 181–189.
- Carlsson, B., Rutgeresson, A. and Smedman, A.-S. 2009. Investigating the effect of a wave-dependent momentum flux in a process oriented ocean model. *Boreal Environ. Res.* **14**, 3–17.
- Charnock, H. 1955. Wind stress on a water surface. *Q. J. R. Meteorol. Soc.* **81**, 639–640.
- Donelan, M. A. 1990. Air-sea interaction. In: *The Sea: Ocean Engineering Science* Volume 9 (eds. B. LeMehaute and D. Hanes). John Wiley, New York, 239–292.
- Donelan, M. A., Hamilton, J. and Hui, W. H. 1985. Directional spectra of wind-generated waves. *Phil. Trans. R. Soc. Lond. A* **315**, 509–562.
- Doyle, J. D. 1995. Coupled ocean wave/atmosphere mesoscale model simulations of cyclogenesis. *Tellus* **47A**, 766–778.
- Doyle, J. D. 2002. Coupled atmosphere-ocean wave simulations under high wind conditions. *Mon. Wea. Rev.* **130**, 3087–3099.
- Drennan, W. M., Graber, H. C. and Donelan, M. A. 1999. Evidence for the effects of swell and unsteady winds on marine wind stress. *J. Phys. Oceanogr.* **29**, 1853–1864.
- Drennan, W. M., Graber, H. C., Hauser, D. and Quentin, C. 2003. On the wave age dependence of wind stress over pure wind seas. *J. Geophys. Res.* **108**, FET10.1–FET10.13, doi:10.1029/2000JC000715.
- Edson, J. B. and Fairall, C. W. 1998. Similarity relationships in the marine atmospheric surface layer for terms in the TKE and scalar variance budgets. *J. Atmos. Sci.* **55**, 2311–2328.
- Fairall, C. W., Bradley, E. F., Hare, J. E., Grachev, A. A. and Edson, J. B. 2003. Bulk parameterization of air-sea fluxes: updates and verification for the COARE algorithm. *J. Clim.* **16**, 571–591.
- Grachev, A. A. and Fairall, C. W. 2001. Upward momentum transfer in the marine boundary layer. *J. Phys. Oceanogr.* **31**, 1698–1711.
- Guo Larsén, X. 2003. Climatological characteristics at a marine site in the Baltic Sea Proper. In: *Air-Sea Exchange of Momentum and Sensible Heat over the Baltic Sea, Comprehensive Summaries of Uppsala Dissertations from the Faculty of Science and Technology* Volume 820. Acta Universitatis Upsaliensis, Uppsala, Sweden, 1–23.
- Guo Larsén, X., Makin, V. K. and Smedman, A.-S. 2003. Impact of waves on the sea drag: measurements in the Baltic Sea and a model interpretation. *Glob. Atmos. Ocean Syst.* **9**, 97–120.
- Guo Larsén, X., Smedman, A.-S. and Högström, U. 2004. Air-sea exchange of sensible heat over the Baltic Sea. *Q. J. R. Meteorol. Soc.* **130**, 519–539.
- Haugen, D. A., Kaimal, J. C. and Bradley, E. F. 1971. An experimental study of Reynolds stress and heat flux in the atmospheric surface layer. *Q. J. R. Meteorol. Soc.* **97**, 168–180.
- Holland, J. Z., Chen, W., Almazan, J. A. and Elder, F. C. 1981. Atmospheric boundary layer. In: *IFYGL: The International Field Year for the Great Lakes* (eds. E. J. Aubert and T. L. Richards). NOAA, Ann Arbor, MI, 109–167.
- Högström, U. 1990. Analysis of turbulence structure in the surface layer with a modified similarity formulation for near neutral conditions. *J. Atmos. Sci.* **47**, 1949–1972.
- Högström, U. 1996. Review of some basic characteristics of the atmospheric surface layer. *Bound.-Lay. Meteorol.* **78**, 215–246.
- Högström, U., Sahlée, E., Drennan, W. M., Kahma, K. K., Smedman, A.-S. and co-authors. 2008. Momentum fluxes and wind gradients in the marine boundary layer – a multi-platform study. *Boreal Environ. Res.* **13**, 475–502.
- Hwang, P. A. 2005. Temporal and spatial variation of the drag coefficient of a developing sea under steady wind-forcing. *J. Geophys. Res.* **110**, C07024.1–C07024.6, doi:10.1029/2005JC002912.
- Janssen, P. A. E. M. and Viterbo, P. 1996. Ocean waves and the atmospheric climate. *J. Clim.* **9**, 1269–1287.
- Janssen, P. A. E. M., Doyle, J. D., Bidlot, J., Hansen, B., Isaksen, I. and co-authors. 2001. Impact and feedback of ocean waves on the

- atmosphere. *ECMWF Technical Memorandum*, no. 341, ECMWF, Reading, England, 32 pp.
- Johansson, C., Smedman, A.-S., Bergström, H., Gryning, S.-E. 2003. Influence of boundary layer height on turbulence structure in the marine atmospheric surface layer over the Baltic Sea. In: *Influence of External factors on the Turbulence Structure in the Boundary Layer, Comprehensive Summaries of Uppsala Dissertations from the Faculty of Science and Technology* Volume 792. Acta Universitatis Upsaliensis, Uppsala, Sweden, 1–29.
- Jones, C. G., Willén, U., Ullerstig, A. and Hansson, U. 2004. The Rossby Centre regional atmospheric climate model Part I: model climatology and performance for the present climate over Europe. *Ambio* **33**, 199–210.
- Large, W. G. and Pond, S. 1981. Open ocean momentum flux measurements in moderate to strong winds. *J. Phys. Oceanogr.* **11**, 324–336.
- Lionello, P., Malguzzi, P. and Buzzi, A. 1998. Coupling between the atmospheric circulation and the ocean wave field: an idealized case. *J. Phys. Oceanogr.* **28**, 161–177.
- Ohlson, A. 2006. *The accuracy of the wind stress over ocean of the Rossby Centre Atmospheric model (RCA)*. Master Thesis. Department of Geosciences, Uppsala University, Sweden, 29 pp.
- Pan, J., Wang, D. W. and Hwang, P. A. 2005. A study of wave effects on wind stress over the ocean in a fetch-limited case. *J. Geophys. Res.* **110**, C02020.1–C02020.15, doi:10.1029/2003JC002258.
- Paulson, C. A. 1970. The mathematical representation of wind speed and temperature profiles in the unstable atmospheric surface layer. *J. Appl. Meteorol.* **9**, 857–861.
- Pierson, W. J. 1964. The interpretation of wave spectrums in terms of the wind profile instead of the wind measured at a constant height. *J. Geophys. Res.* **69**, 5191–5203.
- Pierson, W. J. and Moskowitz, L. 1964. A proposed spectral form for fully developed seas based on the similarity theory of S. A. Kitaigorodskii. *J. Geophys. Res.* **69**, 5181–5190.
- Rutgersson, A. and Sullivan, P. P. 2005. The effect of idealized water waves on the turbulent structure and kinetic energy budgets in the overlying airflow. *Dyn. Atmos. Oceans* **38**, 147–171.
- Rutgersson, A., Smedman, A.-S. and Högström, U. 2001. Use of conventional stability parameters during swell. *J. Geophys. Res.* **106**, 27 117–27 134.
- Rutgersson, A., Carlsson, B. and Smedman, A.-S. 2007. Modelling sensible and latent heat fluxes over sea during unstable, very close to neutral conditions. *Bound.-Lay. Meteorol.* **123**, 395–415.
- Smedman, A.-S., Tjernström, M. and Högström, U. 1994. The near-neutral marine atmospheric boundary layer with no surface shearing stress: a case study. *J. Atm. Sci.* **51**, 3399–3411.
- Smedman, A.-S., Högström, U., Bergström, H., Rutgersson, A., Kahma, K. K. and co-authors. 1999. A case study of air–sea interaction during swell conditions. *J. Geophys. Res.* **104**, 25 833–25 851.
- Smedman, A.-S., Guo Larsén, X., Högström, U., Kahma, K. K. and Pettersson, H. 2003. Effect of sea state on the momentum exchange over the sea during neutral conditions. *J. Geophys. Res.* **108**, 3367, doi:10.1029/2002JC001526.
- Smedman, A.-S., Högström, U., Sahlée, E. and Johansson, C. 2007. Critical re-evaluation of the bulk transfer coefficient for sensible heat over the ocean during unstable and neutral conditions. *Q. J. R. Meteorol. Soc.* **133**, 227–250.
- Stewart, R. W. 1974. The air–sea momentum exchange. *Bound.-Lay. Meteorol.* **6**, 151–167.
- Sullivan, P. P., McWilliams, J. C. and Moeng, C.-H. 2000. Simulation of turbulent flow over idealized water waves. *J. Fluid Mech.* **404**, 47–85.
- Sullivan, P. P., Edson, J. B., Hristov, T. and McWilliams, J. C. 2008. Large-eddy simulations and observations of atmospheric marine boundary layers above nonequilibrium surface waves. *J. Atm. Sci.* **65**, 1225–1245.
- WAMDI Group (Hasselmann, S., Hasselmann, K., Bauer, E., Janssen, P. A. E. M., Komen, G. and co-authors). 1988. The WAM model – a third generation ocean wave prediction model. *J. Phys. Oceanogr.* **18**, 1775–1810.
- Woetmann-Nielsen, N. 1998. Inclusion of free convection and a smooth sea surface in the parameterisation of surface fluxes over sea. *Hirlam Newsletter* **32**: 44–51. Available from: SMHI, SE-601 76 Norrköping, Sweden.